Electronic Supplementary Material (ESI) for Nanoscale Horizons.
This journal is © The Royal Society of Chemistry 2023

Supplementary Information for

Anomalous DNA hybridisation kinetics on gold nanorods revealed via a dual single-molecule imaging and optoplasmonic sensing platform

Narima Eerqing[1,2,†,], Hsin-Yu Wu[1,2,†], Subramanian Sivaraman[1,2], Serge Vincent[1,2], Frank Vollmer[1,2]*

[1]Living Systems Institute, University of Exeter, Stocker Road, Exeter, EX4 4QD, United Kingdom
[2] Department of Physics and Astronomy, University of Exeter, Stocker Road, Exeter EX4 4QL, United Kingdom

†These authors have contributed equally to this work and share first authorship

[*]Email: ne276@exeter.ac.uk

Table of Contents

1. Principle of TIRF-Based Excitation of the WGMs

We proposed a new approach to excite whispering-gallery modes (WGMs) using a commercially available total internal reflection fluorescence (TIRF) objective, as shown in Figure S1a. It is important to understand the near-field distribution and field enhancement at the interface between the superstrate medium (water) and glass substrate when a beam of light is launched from glass to water. Figure S1b shows the simulated and analytical reflectance spectra for *p*- and *s*-polarised illuminations ($\lambda = 785$ nm) as a function of the angle of incidence (θ_i). Total internal reflection (TIR) occurs when θ_i is equal to or greater than the critical angle (θ_c), which is ~ 61.4° for both *p*-polarised and *s*-polarised beams. The corresponding enhancement distributions of the near-field intensity in the surface normal (*z*) direction, in response to *p*- and *s*-polarised incidences, are shown as a function of θ_i in Figure S1c and d, respectively. As θ_i approaches θ_c, the evanescent field is generated at the water-glass interface with a penetration depth rapidly decreasing with increasing θ_i, wherein the maximum field enhancement is about 5.14 times for *p*-polarised illumination. For the *p*-polarised incidence, the continuity of the displacement field across boundaries requires that the normal electric field (E_z) be higher in the lower index material, such that the field enhancement in the water medium immediately adjacent

to the interface is greater than that produced in the *s*-polarised case. Since the refractive index of a glass microsphere is higher than that of water, causing the local effective refractive index to be slightly higher than the background refractive index (n=1.33), the coupling angle at which WGMs are evanescently excited is usually slightly larger than the calculated θ_c.

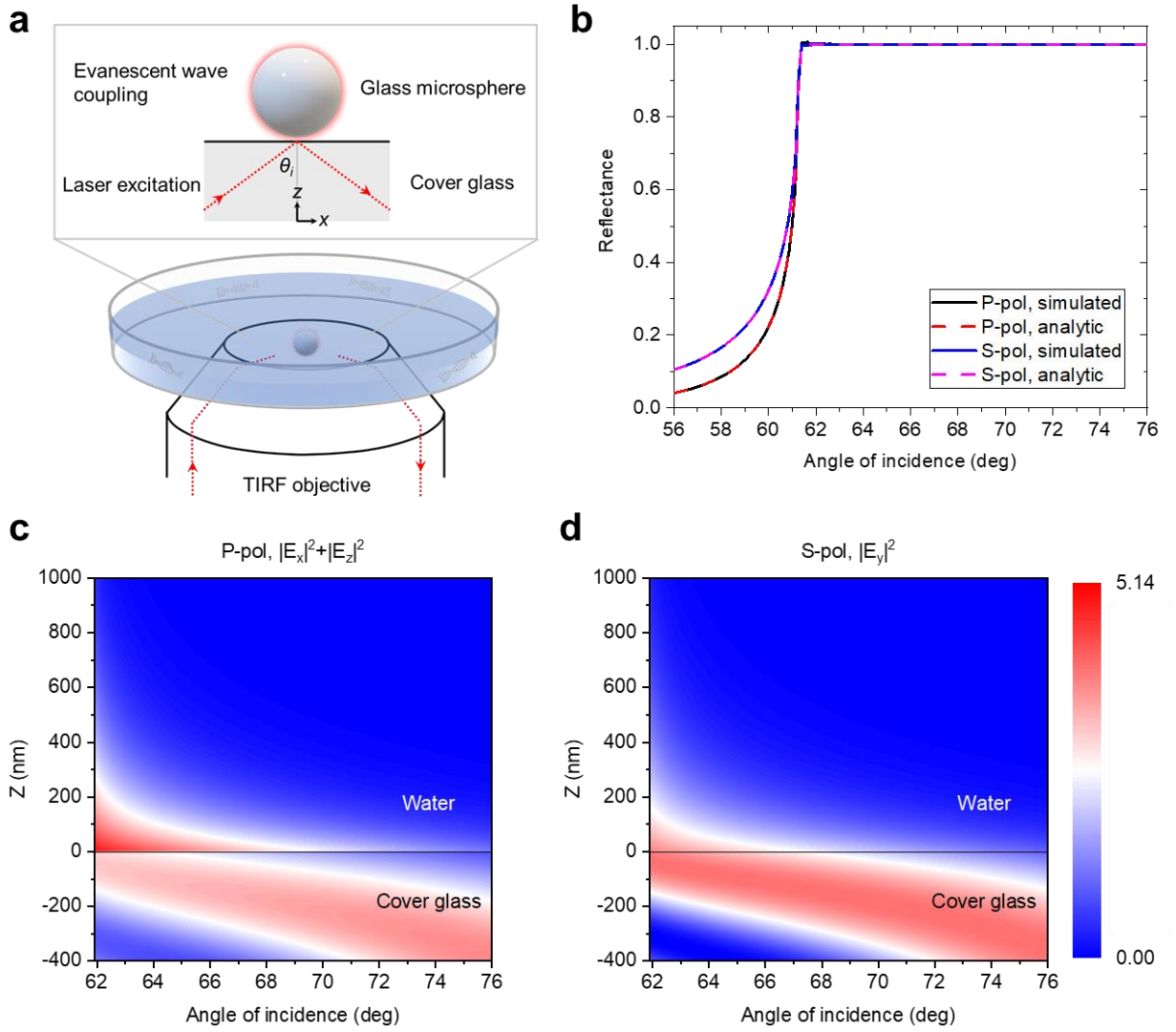

Figure S1. Principle of TIRF-based excitation of the WGMs. (a) Schematic of the objective-based excitation of whispering-gallery modes (WGMs). (b) Simulated and analytical reflectance spectra for a *p*- and *s*-polarised plane wave incident on the water-glass interface from the glass side. (c) and (d) are the corresponding enhancement distributions of the near-field intensity in the surface normal direction for *p*- and *s*-polarised illuminations. The color bar on the right side is scaled by the normalisation of the local electric field intensity ($|\boldsymbol{E}|^2$) to the incident electric field intensity ($|\boldsymbol{E}_{\mathrm{inc}}|^2$).

2. Control Measurements by Refunctionalising the Docking Strands

To verify whether the observed anomalous behavior was a result of hot electron cleaving of *Au-S* bonds, we conducted control experiments through the following procedure:

1) We fabricated the samples (microsphere/coverslip) and immobilised GNRs on the glass surface. GNRs were functionalised with docking DNA and left to interact with imager strands for more than 6 hours.
2) We removed the solution in the chamber cell and rinsed with milliQ water three times, then added the docking DNA with pH≈3 citrate buffer to the chamber. Docking strands were left in the chamber for over 2 hours to fully saturate the surface.
3) We rinsed the chamber three times and added pH≈7 HEPES buffer with 10 mM NaCl to conduct DNA-PAINT measurements. This experiment was carried out using both optoplasmonic sensing and DNA-PAINT techniques.

As reported previously [1], step signals appear on $\Delta\lambda$ traces in the process of docking DNA binding on bare GNRs. We do not, however, observe any step signal within this refunctionalisation process. Figure S2a shows an example trace where the $\Delta\lambda(t)$ response is flat, indicating that the surface is not vacant and instead fully saturated by docking strands. No refunctionalising takes place here on the GNR surfaces. This finding is contrary to Sabrina *et al*. hot electron cleaving experimental results [2]. During imager strand interactions, we were only able to observe a binding step signal and 1 spike signal afterwards, with no signals for the remaining 30 min. This suggests that the event rate was not restored. The same protocol is applied to the DNA-PAINT experiments and as expected, no restored rate was found.

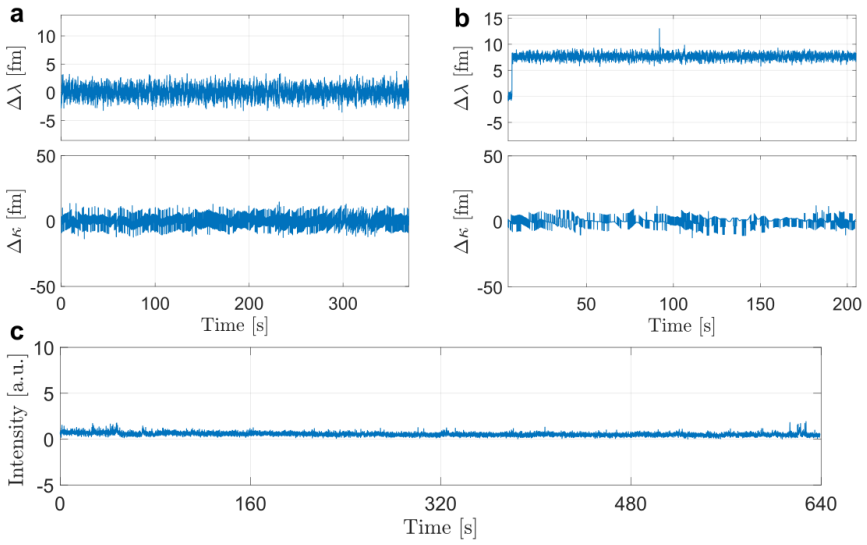

Figure S2 Control measurements for refunctionalisation of T22 docking strands. (a) Refunctionalisation trace for a T22 docking strand monitored via the optoplasmonic sensor. (b) DNA hybridisation trace after T22

refunctionalisation, with the presence of 2 μM ImT22* monitored via the optoplasmonic sensor. (c) DNA-PAINT intensity trace on top of the GNR, lacking rate restoration.

3. Simulation of Plasmonic Heating

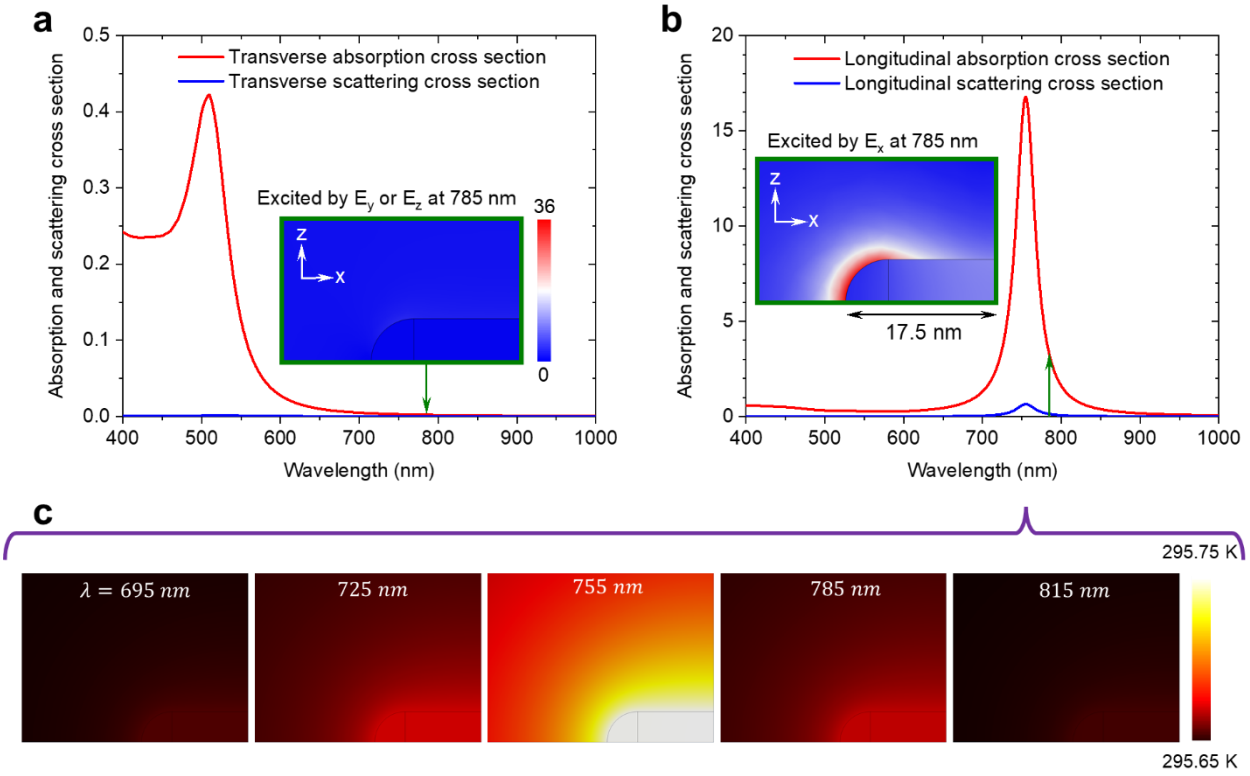

Figure S3. Cross sections and photothermal effects of a gold nanorod in water. Absorption and scattering cross sections of a gold nanorod with a diameter of 10 nm and a length of 35 nm for an incident plane wave propagating along the positive z-direction. The electric field is aligned with (a) the minor and (b) major axes of the nanorod. Insets show the corresponding enhancement distributions of the near-field intensity at the laser excitation wavelength ($\lambda = 785$ nm). Owing to its symmetry, only one quarter of the nanorod is modeled. The color bar is scaled by normalisation of the local electric field intensity ($|\boldsymbol{E}|^2$) to the incident electric field intensity ($|\boldsymbol{E}_{\mathrm{inc}}|^2$). (c) Wavelength-dependent temperature distribution maps associated with the dissipative losses of absorption in the nanorod (b). The maximum temperature difference of 0.1 K occurs at the absorption peak wavelength of 755 nm.

COMSOL Multiphysics is used to calculate the absorption and scattering cross sections of a GNR in water and the results coincide with the vendor's datasheet. Absorption and scattering cross sections are defined as $C_{abs} = \frac{W_{abs}}{I_{inc}A}$ and $C_{sca} = \frac{W_{sca}}{I_{inc}A}$, where I_{inc} is the intensity of the incident field (79.58 W/cm^2), A is the cross-sectional area of the nanorod, and W_{abs} and W_{sca} are respectively the net energy dissipated by the absorbing GNR and scattered across an imaginary spherical surface centered on the GNR. Owing to its symmetry, only one quarter of the GNR is modeled. Photothermal heating (T) is solved via the heat transfer model $\nabla \cdot (-K\nabla T) = Q$, where K is the thermal conductivity,

∇T is the spatial temperature gradient, and Q is the heat source that accounts for power dissipation density due to the light absorption by the GNR. The simulation results show that the maximum temperature change of 0.1K occurs at the absorption peak wavelength of 755 nm under the condition of plane wave incidence in a water host medium. Considering that in reality the GNR is placed onto the surface of the coverslip where TIRF excitation offers the maximum near-field enhancement of a factor of 5 at λ = 785 nm (as shown in Figure S1), the estimated temperature gradient near the surface of the GNR won't be higher than 0.5K.

4. Control Measurements by External Heating

The heating experiments are carried out as follows: A hotplate is used to heat a beaker that is filled with milliQ water. 20mM HEPES buffer with NaCl solution is mixed with and without 40nM imager strands IMP1* in different Eppendorfs separately, all of them are immersed in the beaker. A thermometer is inserted into the beaker to characterise the temperature. We use the coverslip sample acquired using the protocol described in **Supplementary 2**. Before doing the experiments, HEPES buffer with 10mM NaCl is used to rinse the chamber 10 times, each time last for 3minutes. This process is to make sure the temperature of the chamber is constant and to avoid heat loss. Thereby the DNAs on the surface of GNRs are heated to the target temperature (60°C and 80°C). We then conducted two sets of DNA-PAINT experiments, one is carried out under high temperature (60°C and 80°C), the other is using plain buffer to heat to target temperature (60°C and 80°C), and then cooled down to room temperature to conduct DNA-PAINT measurements:

1) DNA-PAINT at high temperatures are conducted by adding the 40nM imagers into the chamber, and measured for 60 °C and 80°C respectively, the results are shown in Figure S4a, c.

2) Cooled to room temperature DNA-PAINT experiments are carried out using the sample described in 2), instead of doing experiments at a high temperature. We heated the chamber using plain buffer, cooled until room temperature and then conduct DNA-PAINT experiments, results shown in Figure S4b, d.

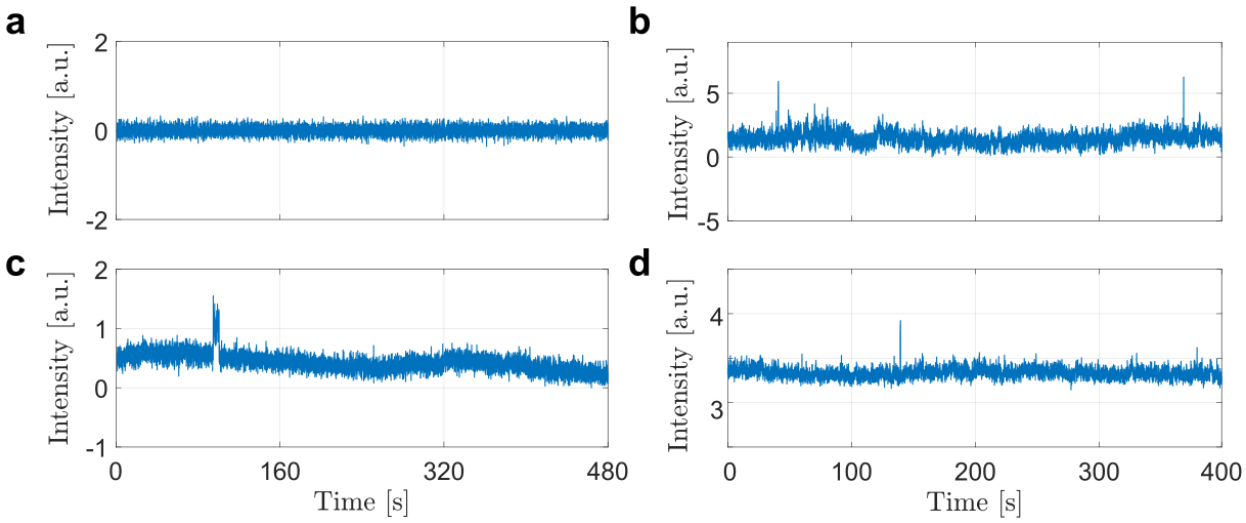

Figure S4 Control measurement with external heating. The intensity time trace shows the DNA-PAINT experiment with 40 nM ImP1*D in (a) 60 °C HEPES buffer, then (c) 80°C HEPES buffer. (b) Heated to 60 °C then cooled to 22.5 °C, and (d), Heated to 80 °C then cooled to 22.5°C.

5. Background Measurements of DNA-PAINT and Optoplasmonic Sensing Systems

The background noise for the optoplasmonic sensing platform is measured after the assembly of the microsphere and GNRs. The average noise is around 2 fm (See Figure S5a). Since the optoplasmonic sensing platform is sensitive to pressure and temperature changes, there would normally be a background trend. We remove this contribution via in-house MATLAB software [3]. The assembly of the optoplasmonic sensor requires coupling between resonant GNRs and the WGM microsphere. GNRs could trigger an irreversible absorption reaction in the pH≈1.6 acidic solution, and this process can be real-time monitored by tracking $\Delta\lambda$ and $\Delta FWHM$ traces. Figure S5b shows typical step signals acquired from the GNR binding process. We observe step signals in both $\Delta\lambda$ and $\Delta FWHM$ traces.

Figure S5c shows the background noise level of the DNA-PAINT technique. When the GNRs are bound to the coverslip surface (with the binding protocol as described above), photoluminescence signals can be seen from the camera. The intensity of a 5x5 ROI corresponding to the GNR location can then be tracked, with Figure S5d showing a typical intensity time trace for that GNR.

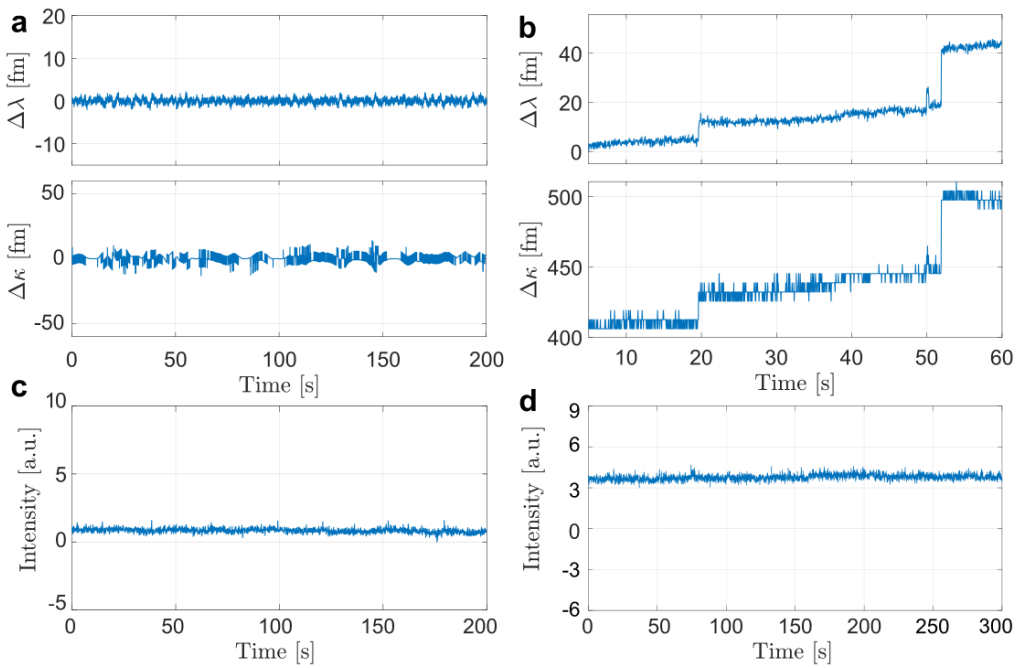

Figure S5 (a) Detrended background noise for optoplasmonic sensing. (b) Real-time binding of GNRs. (c) Background noise for DNA-PAINT in a 5x5 ROI. (d) Intensity trace for a GNR positioned within the 5x5 ROI.

6. Visualising Real-Time DNA Interactions via Optoplasmonic Sensing

In the binding of docking DNA procedure, steps signals can be detected in the $\Delta\lambda$ trace. The positive shift is a result of the change in polarisability/refractive index when immobilising docking stands to the GNR surface. There is, however, no corresponding change in the case of the $\Delta FWHM$ trace. Different from the observation of the GNR binding signals, where a large change in both $\Delta\lambda$ and $\Delta FWHM$ traces exists, single-molecule experiments only exhibit signals pre-dominantly in the $\Delta\lambda$ trace (i.e. $\Delta FWHM$ remains unchanged). The wavelength-shift signal changes for attaching the gold nanorods are that of the plain dielectric microsphere cavity. The wavelength-shift signal changes recorded for singe DNA oligonucleotide molecules are that of the optoplasmonic microcavity which enhances the single-molecule signals at the tips of the nanorods where the plasmon near field intensity is highest, see Ref [5, 6] for details of the different signal transduction mechanisms. In addition, since only sharp binding steps are observed, indicating there are no unspecific ssDNA absorption, otherwise the absorbed ssDNA will wag in the nearfield and detected by the sensor.

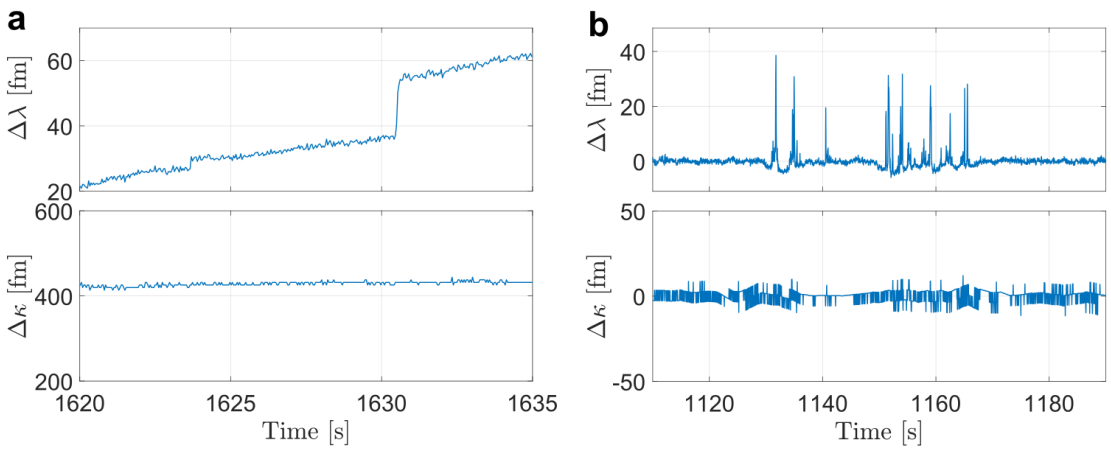

Figure S6 Typical optoplasmonic sensing trace for (a) docking DNA binding to a GNR and (b) transient DNA interactions between docking and imager strands.

Figure S6b shows an example of a transient DNA interactions trace, where no $\Delta FWHM$ is observed while only spike-like signals emerge.

7. Example of Single-Molecule Localisation

Figure S7a shows a single frame of a DNA-PAINT image at the GNR position, where a single-molecule localisation microscopy algorithm named ThunderSTORM [4] is applied to estimate the sub-pixel location of the single molecule.

Figure S7b is an intensity time trace acquired from a 5×5 ROI (yellow box in Figure S7a), and the signal marked by the red star corresponds to the crosshair mark in Figure S7a. By stacking these locations one can eventually reconstruct super-resolution images of the GNR geometry.

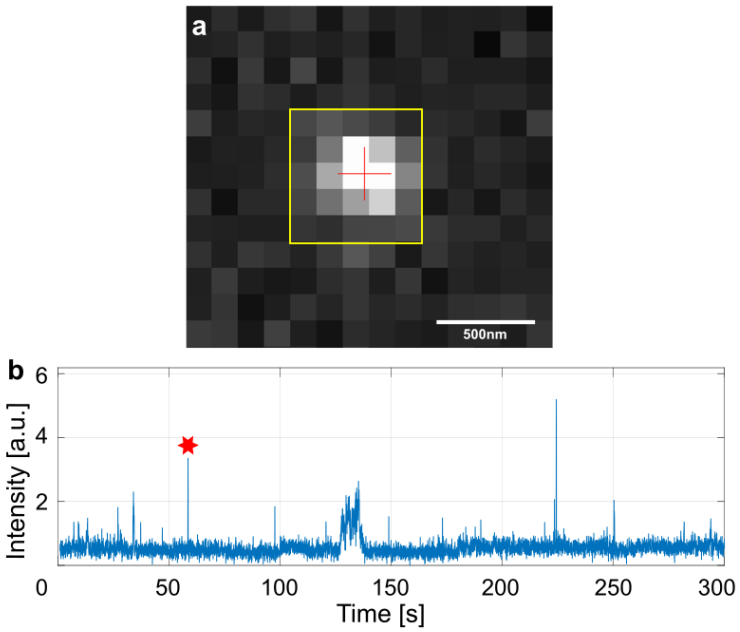

Figure S7 Individual frame of a DNA-PAINT image on top of a single GNR, where (a) shows the localisation of the transient interaction corresponding to (b) the red starred timepoint in the trace.

8. Spike events extraction and analysis

The spike events are extracted from both intensity (DNA-PAINT) and wavelength shift (optoplasmonic sensing) traces with similar protocol. In the case of optoplamonic sensing, there is normally a non-constant background signal, originating from a long-term drift caused by comparably slow changes of environmental attributes like pressure and temperature. While for DNA-PAINT the background signals are generally flat. Figure S8a shows an example of optoplasmonic sensing data trace with a background. The first step is to remove the background trending using custom MATLAB code [3]. Figure S8b shows the detrended trace. The standard deviation σ is taken over the background intervals of this trace, where we then use a threshold of 4σ to extract the spike events. Figure S8c shows the spike events detected after applying a threshold filter.

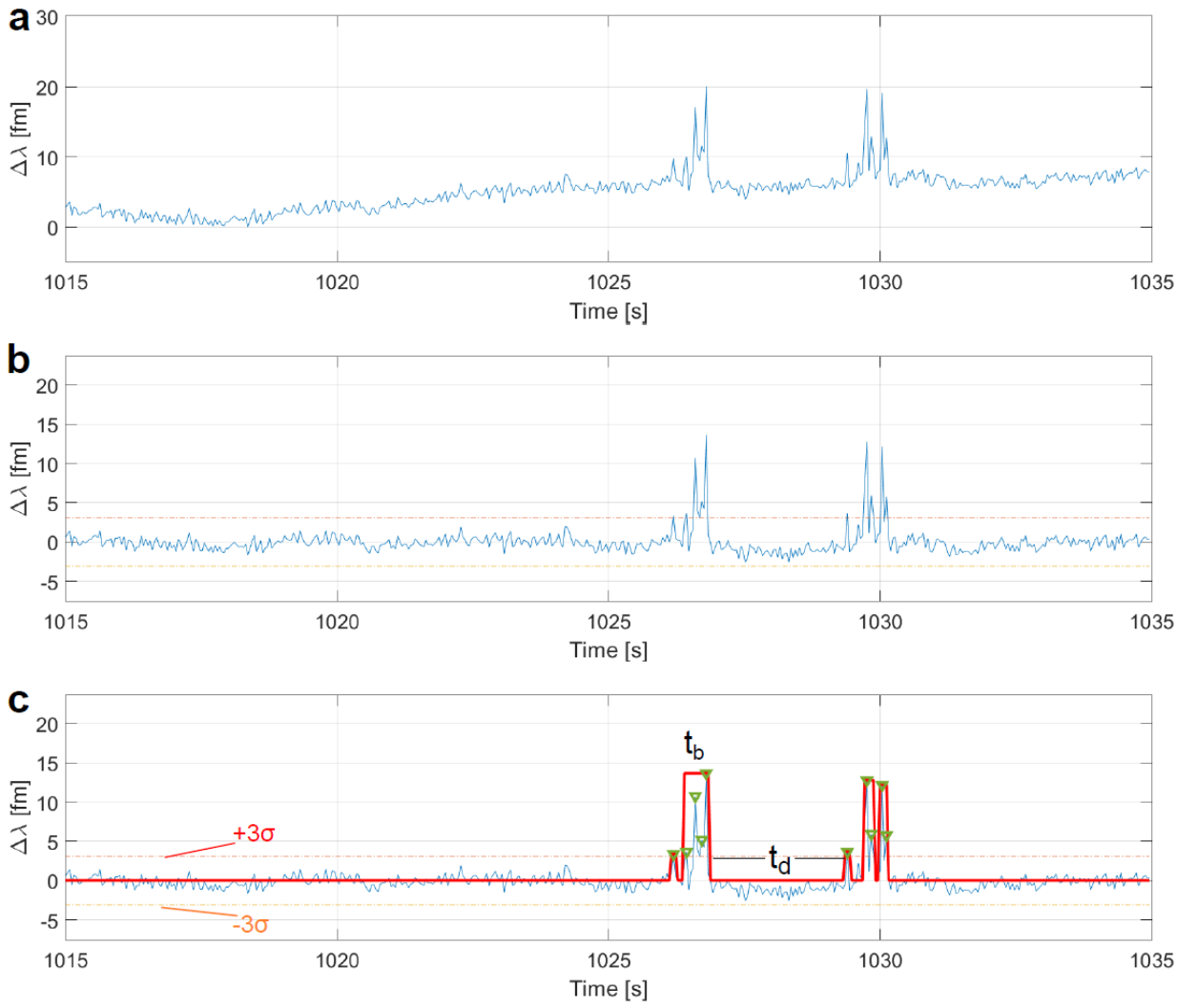

Figure S8 Illustration of the spike extraction process. (a) Original background data trace. (b) Background-free data trace acquired with custom detrending algorithms. (c) The spike events detected after applying a threshold filter.

9. Detailed process for DNA-PAINT and optoplasmonic sensing

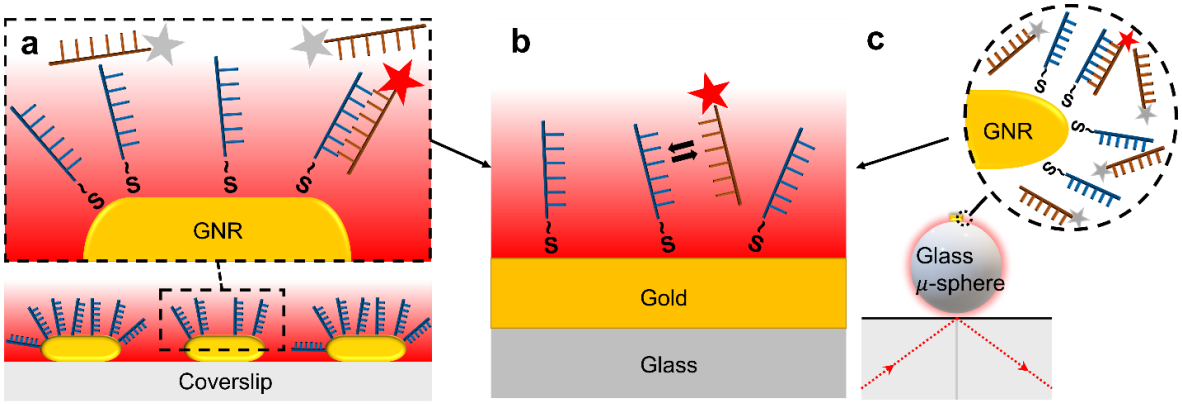

Figure S9 Detailed schematic process for (a) DNA-PAINT and (c) optoplasmonic sensing (b) shows that in both experiments the reaction along the surface is the same, where docking strands are immobilised on the gold surface, and the imagers are transiently interacting with the docking strands. The imagers denoted by the red star provide signals.

10. Control measurements with unrelated sequences

Here we show the data from two sets of non-complementary sequences. The sequences are listed in the following table.

ssDNA	Sequence (5'-3')
UnrelatedP1*D	[DY782] TAT TTC TAC A
UnrelatedP1*	TAT TTC TAC A
UnrelatedT22*D	[DY782] GAG ATA AAC GAG AAG GAT TGA T
UnrelatedT22*	GAG ATA AAC GAG AAG GAT TGA T

Table S1. Sequences of unrelated DNA strands used in the control measurements.

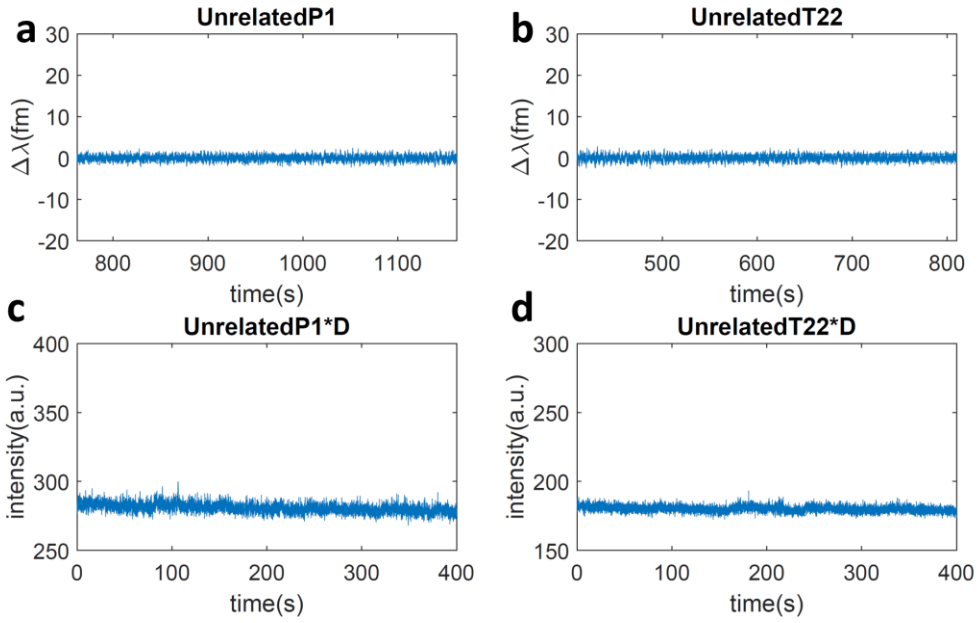

Figure S10 Control measurement of unrelated DNA strands. (a,b) Intensity trace of WGM signals of unrelated DNA P1 and T22 strands without DY782. (c,d) DNA-PAINT experiments for unrelated P1 and T22 strands attached with DY782, respectively.

We observed no signals from each control measurement, indicating that no unspecific interactions were involved.

11. More data showing the different NaCl concentration effect.

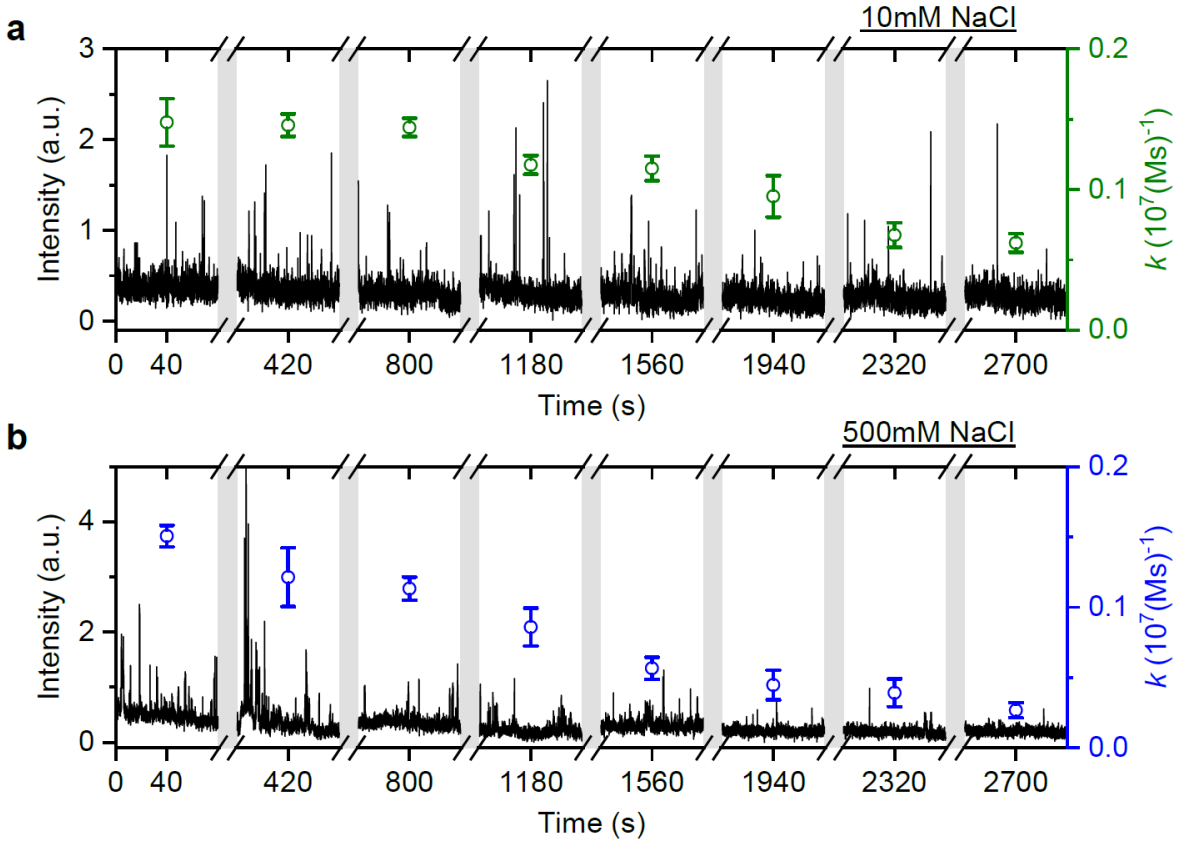

Figure S11 The DNA-PAINT measurements with 20nM ImT22*D. The experiments are conducted with (a) 10mM NaCl HEPES buffer and (b) 500mM NaCl HEPES buffer. The event rates are plotted accordingly.

12. References

[1] Baaske, M. D., Foreman, M. R., & Vollmer, F. (2014). Single-molecule nucleic acid interactions monitored on a label-free microcavity biosensor platform. Nature nanotechnology, 9(11), 933-939.

[2] Simoncelli, S., Li, Y., Cortés, E., & Maier, S. A. (2018). Nanoscale control of molecular self-assembly induced by plasmonic hot-electron dynamics. *ACS nano*, *12*(3), 2184-2192.

[3] Subramanian, S., Kalani Perera, K. M., Pedireddy, S., & Vollmer, F. (2022). Optoplasmonic Whispering Gallery Mode Sensors for Single Molecule Characterization: A Practical Guide. In Single Molecule Sensing Beyond Fluorescence (pp. 37-96). Springer, Cham.

[4] Ovesný, M., Křížek, P., Borkovec, J., Švindrych, Z., & Hagen, G. M. (2014). ThunderSTORM: a comprehensive ImageJ plug-in for PALM and STORM data analysis and super-resolution imaging. Bioinformatics, 30(16), 2389-2390.
[5] Yu, D., Humar, M., Meserve, K. et al. Whispering-gallery-mode sensors for biological and physical sensing. Nat Rev Methods Primers 1, 83 (2021).
[6] Subramanian, S., Kalani Perera, K.M., Pedireddy, S., Vollmer, F. (2022). Optoplasmonic Whispering Gallery Mode Sensors for Single Molecule Characterization: A Practical Guide. In: Bowen, W., Vollmer, F., Gordon, R. (eds) Single Molecule Sensing Beyond Fluorescence . Nanostructure Science and Technology. Springer, Cham.